ELSEVIER

Soil Dynamics and Earthquake Engineering 27 (2007) 541–552

SOIL DYNAMICS AND EARTHQUAKE ENGINEERING

www.elsevier.com/locate/soildyn

Effect of lateral heterogeneity on surface wave testing: Numerical simulations and a countermeasure

Chih-Ping Lin*, Chun-Hung Lin

Department of Civil Engineering, National Chiao Tung University, Hsinchu, Taiwan

Received 7 June 2006; received in revised form 24 October 2006; accepted 25 October 2006

Abstract

The surface wave (S-wave) method has gained popularity in engineering practice for determining S-wave velocity depth profiles. A growing trend is towards the application of S-wave testing for spatially 2-D S-wave velocity tomography, ignoring the assumption of horizontally layered medium. A fourth-order velocity-stress finite difference method is used to perform numerical simulations of S-wave testing in earth models with lateral variation. Results show that the lateral heterogeneity induces a non-stationary property in the space domain, resulting in false depth-related dispersion or higher modes if conventional approach based on stationary assumption is used for the dispersion analysis. Artifacts maybe introduced in spatially 2-D S-wave velocity imaging if the effect of lateral heterogeneity is not accounted for. As a potential countermeasure, a high-lateral-resolution S-wave method is proposed to reduce the effect of lateral heterogeneity while maintaining the resolution and depth range of dispersion analysis. It consists of a walk-away survey and a phase-seaming procedure when synthesizing seismograms with different nearest source-to-receiver offset, allowing wide-wavelength dispersion analysis within a small spatial range. The proof of concept is given with several numerical examples. They show that the high-resolution S-wave method can greatly alleviate the effect of lateral heterogeneity and increase spatial resolution.

Keywords: Surface wave; Multi-channel analysis of surface wave; Lateral heterogeneity

1. Introduction

Seismic surface wave (S-wave) profiling is gaining popularity in engineering practice for determining shear-wave velocity profile [1,2]. The main advantage of S-wave methods is essentially related to its non-destructive and non-invasive nature that allows the characterization of hard-to-sample soils without the need for boreholes that makes the subsurface seismic methods (such as down-hole and cross-hole methods) expensive and time consuming. S-wave testing is not affected by sample disturbance or insertion effects and is capable of sampling a representative volume of the ground even in difficult materials such as fractured rock or gravelly deposit. Based on the S-wave velocity profile or spectral amplitude obtained from S-wave testing, the method has been successively applied to various problems, such as profiling sub-ground stiffness [3], delineating potential liquefaction area [4], evaluating thickness and condition of pavement [5,6], evaluating efficiency of soil improvement [7], characterizing waste disposal site [8,9] and detecting underground objects [10].

S-wave methods are based on the dispersive nature of Rayleigh (or Love) waves in vertically heterogeneous media. The variation of S-wave-phase velocity with frequency results from the variation of S-wave velocity with depth. The dispersion curve is experimentally determined from the wave field data related to the propagation of a perturbation generated by a dynamic source and recorded by geophones or accelerometers on the ground surface. A subsequent inversion process, based on the numerical simulation of wave propagation in layered media, leads to an estimate of the S-wave velocity profile. S-wave testing in geotechnical engineering have been for a long time associated to the two-station setup used in the spectral analysis of surface wave (SASW) method [e.g., 11–13]. To improve inherent difficulties in evaluating and distinguishing signal from noise with only a pair of

*Corresponding author. Tel.: +886 3 513 1574; fax: +886 3 571 6257.
E-mail address: cplin@mail.nctu.edu.tw (C.-P. Lin).

0267-7261/$ - see front matter © 2006 Elsevier Ltd. All rights reserved.
doi:10.1016/j.soildyn.2006.10.008

receivers by this method, new techniques incorporating multi-station receivers and 2-D wavefield transformation, named as the multi-station analysis of surface wave (MASW), were developed [e.g., 14–17]. This method simplifies the testing procedure and the data analysis is better automated. While improvements on MASW method are continued to be studied, especially in the inversion phase, engineering applications utilizing MASW method are growing rapidly in recent years. A growing trend is towards the application of MASW for spatially 2-D S-wave velocity imaging [e.g., 4,18–22]. However, S-wave methods assume that the propagation medium is horizontally layered. This assumption is inherent to the inverse problem required during dispersion curve interpretation. Using a 1-D profiling method to map 2-D structure may be justified if the survey line is short relative to the lateral variation. But MASW typically requires long receiver spread in order to have enough depth coverage. The accuracy and lateral resolution of 2-D S-wave velocity imaging by S-wave is questionable.

MASW has been used to map lateral variation of S-wave velocity overlooking the assumption of horizontally layered medium. Little work has been done regarding the effect of lateral heterogeneity on S-wave testing. As a first approach to this problem, finite difference method is used to compute synthetic seismograms of S-wave testing for two simple earth models with lateral heterogeneity. The effects and implications of lateral heterogeneity on S-wave dispersion are discussed. As a countermeasure, a newly developed method, called high-lateral-resolution S-wave method, is proposed to reduce the effect of lateral heterogeneity. The effectiveness of the countermeasure is assessed by numerical simulations.

2. Methods

2.1. Finite difference simulations of surface wave testing

The 2-D, fourth-order, staggered-grid, velocity-stress finite difference method developed by Levander [23] was used to compute seismograms for earth models with lateral heterogeneity. Instead of using the wave equation which is a second-order hyperbolic system, the staggered-grid, velocity-stress scheme utilizes the equations of motion and Hooke's Law and applies time derivative to Hooke's Law to form a coupled first-order partial differential equations. The scheme is second-order accurate in time and fourth-order accurate in space.

Four boundary conditions need to be specified: one free surface condition and three radiation conditions for simulating the infinite earth. For the free surface, image method [24] is used, in which velocity is simply set equal to zero everywhere above the free surface. For radiation conditions at two sides and bottom, absorbing technique introduced by Cerjan et al. [25] is applied to reduce the reflections from the boundaries. The absorbing technique applies a window function, at each time step, which tapers the amplitudes from 1 to $\geqslant 0.92$ across the boundary zone. The stability condition for the numerical scheme, according to Levander [23], is

$$\Delta t < \frac{6}{7\sqrt{2}} \frac{h}{V_{p\,max}}, \tag{1}$$

where Δt is the time step, h is the grid spacing, and $V_{p\,max}$ is the maximum P-wave velocity. In addition, to minimize the effects of grid dispersion and grid anisotropy, the grid spacing should be smaller than one-fifth of the shortest wavelength of interest,

$$h < \frac{\lambda_{Smin}}{5}, \tag{2}$$

where $\lambda_{S\,min}$ is the shortest (S-wave) wavelength of interest.

Typical experimental configurations are used to simulate the seismograms recorded by MASW tests. The first derivative of the Gaussian function is taken as the normal stress point source applied to the free surface. As a first approach, parametric studies were performed on two simple earth models, one showing a two-layer vertical structure and the other simulating a vertical fault in a near-surface setting. The earth models, although simple, can clearly illustrate the effect of lateral velocity variation on the S-wave dispersion. They are also used to test the performance of the newly proposed countermeasure. Fig. 1 shows the finite difference mesh whereas the parameters used for calculations are listed in Table 1. The study zone is placed at the center of the mesh. Although absorbing boundary has been applied, the size of the mesh is extended to avoid any S-wave reflections from the boundaries within

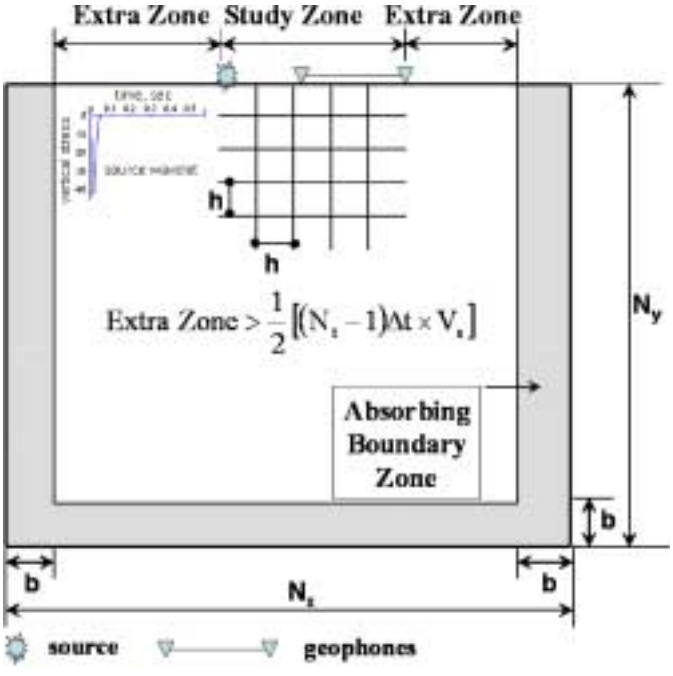

Fig. 1. Illustration of the finite-difference mesh used for computing the synthetic seismograms of surface wave testing.

Table 1
Parameters used for the 2-D finite difference modeling

Parameter	Value
N_x (cells)	1200
N_y (cells)	600
N_t (steps)	4096
h (m)	0.5
Δt (s)	0.00024
Source Wavelet	$g(t) = -2\alpha t \exp(-\alpha t^2)$
α	2500
b (cells)	60

the recording time. Only the vertical components of the velocities at the geophone locations are recorded, thus simulating the typical S-wave testing. The stress–time relation of the source function is also shown in Fig. 1. It is continuous and smooth both in time domain and frequency domain to ensure numerical stability. Changing the parameter of the source function would only affect the frequency content of resulting synthetic seismograms. The small pulse width was used to have a wide frequency bandwidth.

2.2. Analysis of surface wave dispersion

To avoid further complication and uncertainty involved during S-wave velocity inversion, the effect of lateral heterogeneity is investigated on the dispersion characteristics of S-wave. Various algorithms of wavefield transformation exist for analysis of S-wave dispersions, such as p–f (slowness–frequency) transform [26], f–k (frequency–wavenumber) transform [27], and f–v (frequency–velocity) transform [28]. It will be shown that these transforms are equivalent and a unified algorithm is introduced in which the wavefield can be transformed into f–k, f–p, f–v, or f–λ (frequency–wavelength) domain. The algorithm starts with a discrete Fourier transform (DFT) of the multi-station data $u(t_m, x_n)$ in the time domain

$$U(f_i, x_n) = \frac{1}{M}\sum_{m=0}^{M-1} u(t_m, x_n)\exp(-j2\pi f_i t_m), \quad (3)$$

where u is the velocity recorded by the receivers, U is the real part of the DFT of u, $j = \sqrt{-1}$, $t_m = m\Delta t$, $f_i = i\Delta f = i/[(M-1)\Delta t]$, and $x_n = n\Delta x$. The subscripts i, n, and m in Eq. (3) are integer indices to represent respectively discrete points in the frequency, space, and time domain. For each frequency component, the wavefield $U(f_i, x)$ becomes a harmonic function of space. The wavenumber k can be determined from the wavenumber analysis (spectral analysis in space). The wavenumber analysis of the multi-station signals can be performed using the discrete-space Fourier transform

$$Y(f_i, k) = \sum_{n=0}^{N-1} U(f_i, x_n)\exp(-j2\pi k x_n), \quad (4)$$

where $Y(f_i, k)$ represents the wavefield in the frequency–wavenumber domain. For a fixed space coordinate (x), the wavenumber (k) can take positive value or negative value, each representing the forward and backward propagating wave depending on the source location.

The discrete-space Fourier transform is different from the DFT in that the wavenumber remains continuous but the fast algorithm (FFT) cannot be used [29]. The number of receivers is typically much less than the number of samples in the time domain. The discrete-space Fourier transform rather than DFT is used in the space domain, so that the resolution in the wavenumber domain can be arbitrarily chosen. The wavenumber {k} of the S-wave can be identified at the peaks of the amplitude spectrum of $Y(f_i, k)$. The phase velocity is then determined by the definition $v = 2\pi f/k$. Spectra in other domains can be derived from Eqs. (3) and (4) by simply changing the variable $k = 2\times\pi fp$ for the frequency–slowness domain, $k = 2\times\pi f/v$ for the frequency–velocity domain, or $k = 2\times\pi f/\lambda$ for the frequency–wavelength domain. For example, the frequency–velocity (f–v) transform can be obtained as

$$Y(f_i, v) = \sum_{n=0}^{N-1} U(f_i, x_n)\exp\left(-j\frac{2\pi f_i}{v}x_n\right), \quad (5)$$

where $Y(f_i, v)$ represents the wavefield in the frequency–velocity domain. This algorithm is used to process the synthetic seismograms and the amplitude spectrum of the 2-D transform is presented in f–v domain.

3. Results and discussion

3.1. Effect of lateral heterogeneity

Fig. 2a depicts a simplified earth model used to generate a seismogram to illustrate the effect of lateral heterogeneity. The earth model consists of two vertical layers. The S-wave velocity of the softer material to the left is 260 m/s and the stiffer material to the right has a S-wave velocity equal to 530 m/s. Seventy geophones with 1-m interval are spread out at the vertical interface. The resultant seismogram, shown in Fig. 2b, reveals two apparent phenomena. The distance-arrival time curve to the left and right of the vertical interface has distinct slopes and the geophones to the left of the vertical interface records backward-propagated reflected waves. By taking Fourier transforms of the wavefield $u(t_m, x_n)$ with respect to time (i.e. applying Eq. (3)), Fig. 2c presents the spectral amplitude of $U(f_i, x_n)$ as a function of frequency and source-to-receiver offset. The predominant frequencies are similar at both sides, but the amplitude spectra at the left side of the vertical interface has a oscillated feature due to the interference of reflected waves. Therefore, the spectral amplitude $U(f_i, x_n)$ may serve as a simple tool to detect presence of lateral variation. Fig. 2d shows the real part of the transformed wavefield $U(f_i, x_n)$ as a function of

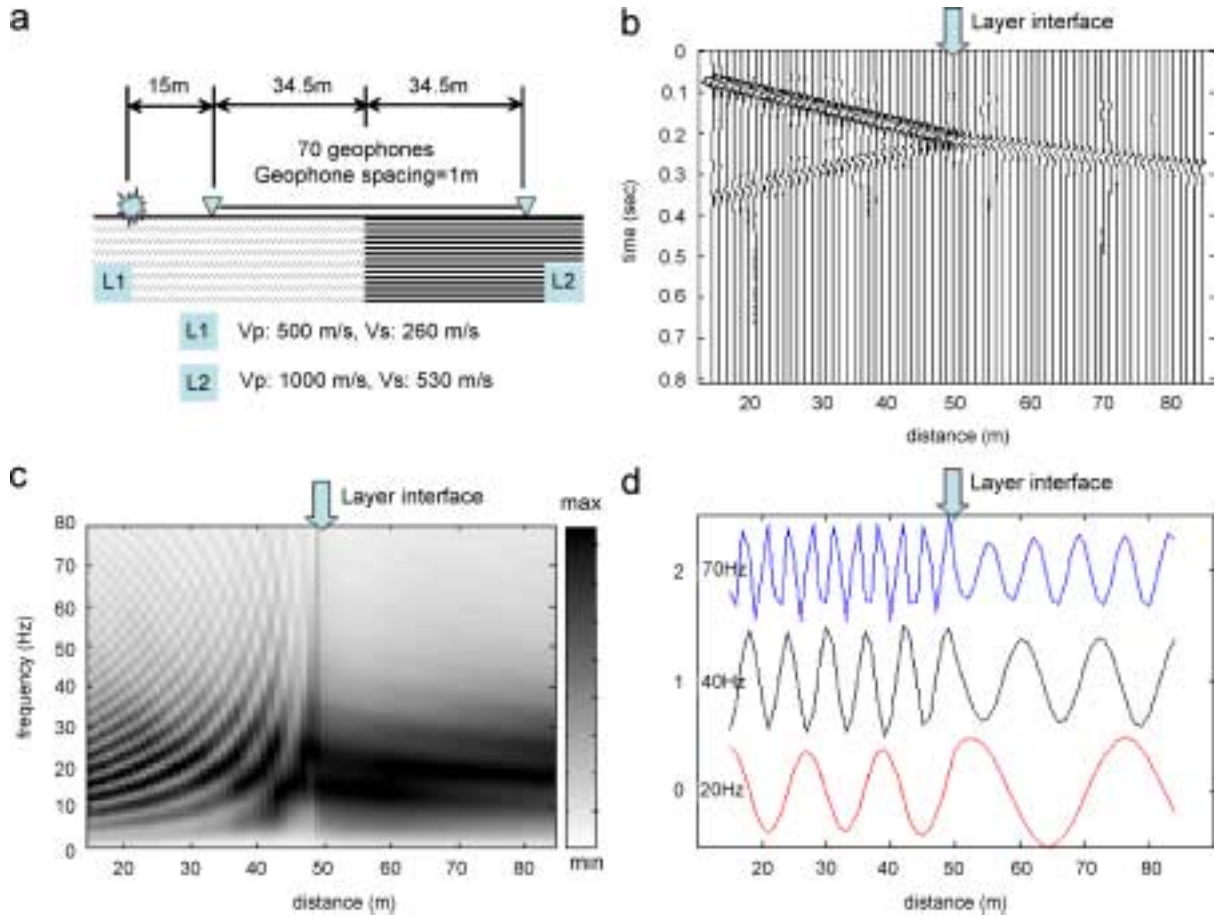

Fig. 2. A simple example illustrating the effect of lateral heterogeneity on surface wave testing (a) two-layer vertical structure representing a simplified case of lateral variation in elastic properties, (b) synthetic seismogram of surface wave testing, (c) spectral amplitude as a function of frequency and source-to-receiver offset, (d) real part of the transformed wavefield as a function of source-to-receiver offset at three frequencies components (20, 40, and 70 Hz).

source-to-receiver offset for three frequency components (20, 40, and 70 Hz). Apparently, the signal to the left of the vertical interface integrates the forward and backward propagating waves with a shorter wavelength, while the signal to the right of the vertical interface shows a forward-propagating wave with a longer wavelength. Fig. 2d clearly reveals that the lateral heterogeneity induced non-stationary property in the space domain. As a consequence, the wavelength of S-wave is not only a function of frequency but also a function of source-to-receiver offset.

If only 24 geophones are used in the field for data acquisition, as is the case for many practical applications, the dispersion analysis is expected to depend on the location of the geophone spread. Fig. 3 shows the f–v amplitude spectra for three different locations of geophone spread near the vertical interface. The non-stationary property due to lateral heterogeneity results in "false" dispersion or higher modes if conventional approach based on stationary assumption is used for dispersion analysis. The degree of influence on the dispersion curve depends not only on the location of the geophone spread but also on the frequency or wavelength, with lower frequency (i.e. higher wavelength) component deviating from uniform dispersion more. When making the horizontally layered assumption during inversion as usual, the lateral variation of S-wave velocity will be falsely recognized as the vertical variation, hence producing artifacts in 2-D S-wave velocity imaging.

Fig. 4a depicts a two-layer step structure to simulate a vertical fault in a near-surface setting. While the two-layer vertical structure (Fig. 2a) represents a simple case of lateral variation in elastic properties, the two-layer step structure (Fig. 4a) is used to illustrate the effect of lateral variation in layer thickness. The vertical step is located at the center point of a 70-geophone spread. All the modeling parameters are the same as in the two-layer vertical structure. The resulting seismogram, as shown in Fig. 4b, also shows distinct waveforms at different sides of the vertical step. However, no backward-propagated reflected wave can be visualized in the seismogram. The amplitude spectrum in the frequency–space domain (Fig. 4c) reveals a shift in the dominant frequencies. The dominant frequencies increase as the thickness of the first layer (low-velocity layer) decreases. It appears that the first step of the wavefield transformation (Eq. (3)) can be used as a first approach to detect major lateral variation of earth structure within the geophone spread, as shown in Figs. 2c and 4c. Fig. 4d presents the real part of the transformed

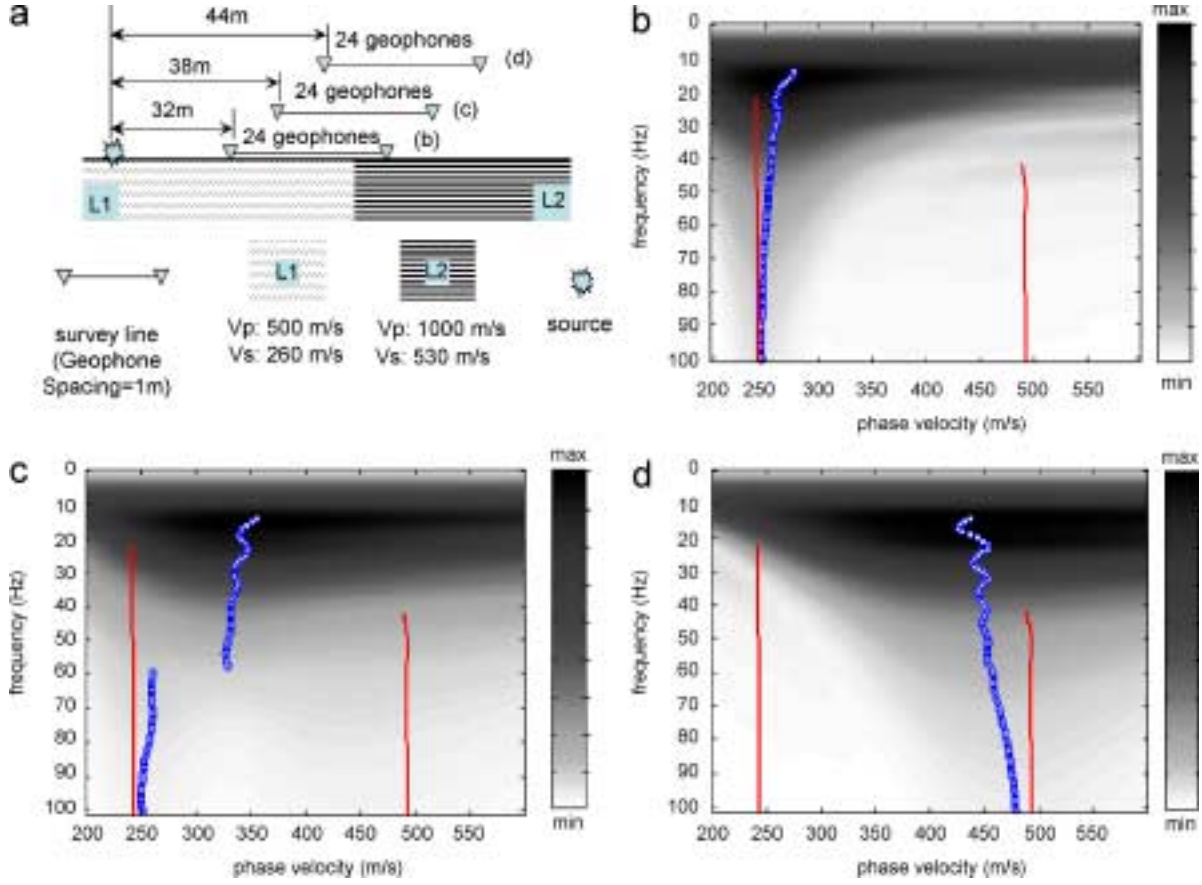

Fig. 3. Effect of lateral heterogeneity on MASW dispersion analysis (a) three cases of geophone spread near the vertical interface of the two-layer vertical structure (b–d) f–v amplitude spectra for each case.

wavefield as a function of source-to-receiver offset for three frequency components (20, 40, and 70 Hz). The signals to the left and right sides of the vertical step have different apparent wavelengths only at lower frequencies, in which the corresponding wavelength is greater than the upper block depth. This is consistent with the fact that the lateral variation takes places only beyond a certain depth. Non-stationary property is manifested when the wavelength is greater than such depth and becomes more obvious with greater wavelength. But the non-stationary property will eventually become weaker as the wavelength becomes significantly larger than the thickness of the top layer since the lower half space remains homogeneous.

Fig. 5 shows the f–v amplitude spectra for three different locations of a conventional 24-geophone spread in the two-layer step structure. The S-wave "samples" the earth with a sampling depth approximately equal to one wavelength. The phase velocity represents some integrated and weighted average of the S-wave velocities within the sampled depth. The sampling weighting for shallow depth is much higher than for deep depth. Hence, the lateral variation in Rayleigh-wave phase velocity is much less dramatic than lateral variation in the first-layer thickness. In such a case, the experimental dispersion curve appears to change smoothly from the case of lower block to upper block. As observed from Figs. 3 and 5, the dispersion curve obtained from the MASW method reflects not only the vertical variation but also the lateral variation in an earth model. Vertical heterogeneity causes frequency dependency while lateral heterogeneity causes space dependency to the Rayleigh-wave velocity. Inherent to the S-wave propagation, variations of Rayleigh-wave velocity in the frequency and space domain are both more sensitive to heterogeneity in shallow depths than in large depths.

3.2. A Countermeasure: high-lateral-resolution surface wave method

The assumption of horizontally layered medium is inherent to the inverse problems required for estimating the S-wave velocity profiles from dispersion curves. The velocity dispersion due to lateral heterogeneity in a MASW test will be misinterpreted as vertical variation of S-wave velocity. To minimize the effect of lateral heterogeneity on the estimation of depth–velocity profile, one might think of reducing the geophone spread. However, the geophone spread in a MASW test should be sufficiently long for two reasons: (a) to reduce spectral leakage and (b) distinguish between fundamental mode and possible higher modes [17]. The wavefield recorded during S-wave testing is truncated by the geophone spread. Consequently, the maximum wavelength where the velocity can be accurately

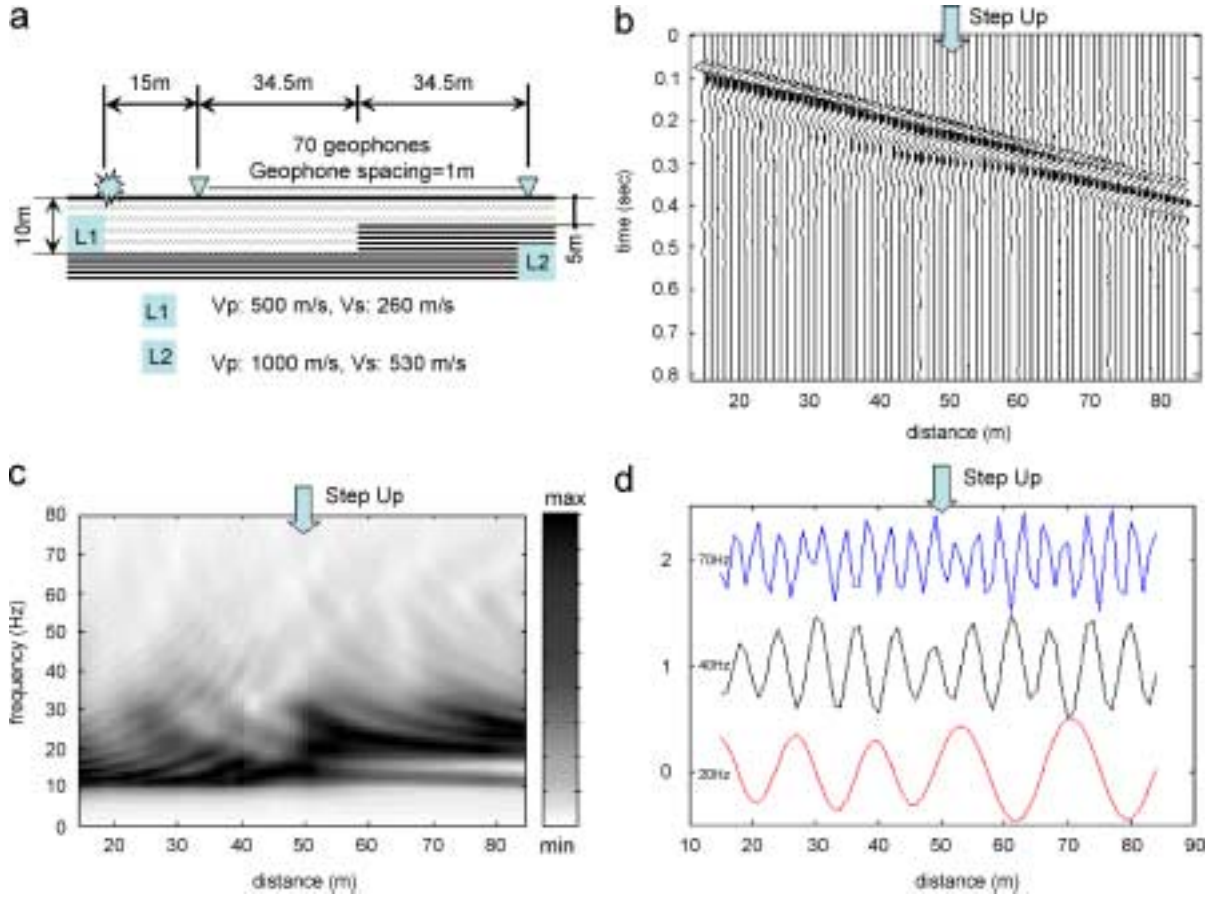

Fig. 4. Example illustrating the effect of lateral heterogeneity on surface wave testing (a) two-layer step structure representing a simplified case of lateral variation in layer thickness, (b) synthetic seismogram of surface wave testing, (c) spectral amplitude as a function of frequency and source-to-receiver offset, (d) real part of the transformed wavefield as a function of source-to-receiver offset at three frequencies components (20, 40, and 70 Hz).

determined is proportional to the geophone spread. For deposits with S-wave velocity varying irregularly with depth, even longer geophone spread may be required to separate fundamental mode from higher mode(s). In a multi-mode S-wave propagation, the experimental dispersion curve obtained from a short geophone spread represents the location-dependent apparent dispersion curve [17], which may be different from modal dispersion curves. Therefore, a long geophone spread is critical to ensure the fundamental modal dispersion curve is correctly obtained. As a consequence, within the long geophone spread in a MASW test, the assumption of horizontally layered medium is often violated.

The non-stationary property in the space domain due to lateral heterogeneity may be analyzed by non-stationary signal processing techniques, such as band-pass filters and wavelet transforms. However, the trade-off between the wavenumber (spatial frequency) and spatial resolution limits its applicability. While a small spatial window is desired for detecting lateral variation with high spatial resolution, good wavenumber resolution requires large spatial window. An alternative countermeasure, named the high-lateral-resolution S-wave method, is proposed to reduce the effect of lateral heterogeneity and increase lateral resolution. It is based on conducting the field survey and collecting the data in a special manner. As an example to explain the high-lateral-resolution S-wave method, Fig. 6 shows a survey line deploying three geophones with spacing Δx, geophone spread L, and nearest source-to-receiver offset X_0. Multiple shots are recorded with shot interval equal to geophone spread L such that the farthest source-to-receiver offset of the preceding shot is equal to the nearest source-to-receiver offset of the subsequent shot. The offset range is initially from X_0 to (X_0+L) when using the conventional multi-station configuration. After three consecutive walk-away shots, all collected field data can be synthesized into one seismic record according to the source-to-receiver offset. The synthesized seismogram has an extended offset range from X_0 to (X_0+3L). If the number of shots is significantly greater than the number of geophones, the shots and geophones can be interchanged to increase the survey efficiency (Fig. 7).

Lateral variation of the stratum might induce static errors when synthesizing seismic records from different shots. For example, Fig. 8a shows a walk-away test on the two-layer vertical structure. Although, the last trace of the first shot and the first trace of the second shot have the same source-to-receiver offset, they have different phase

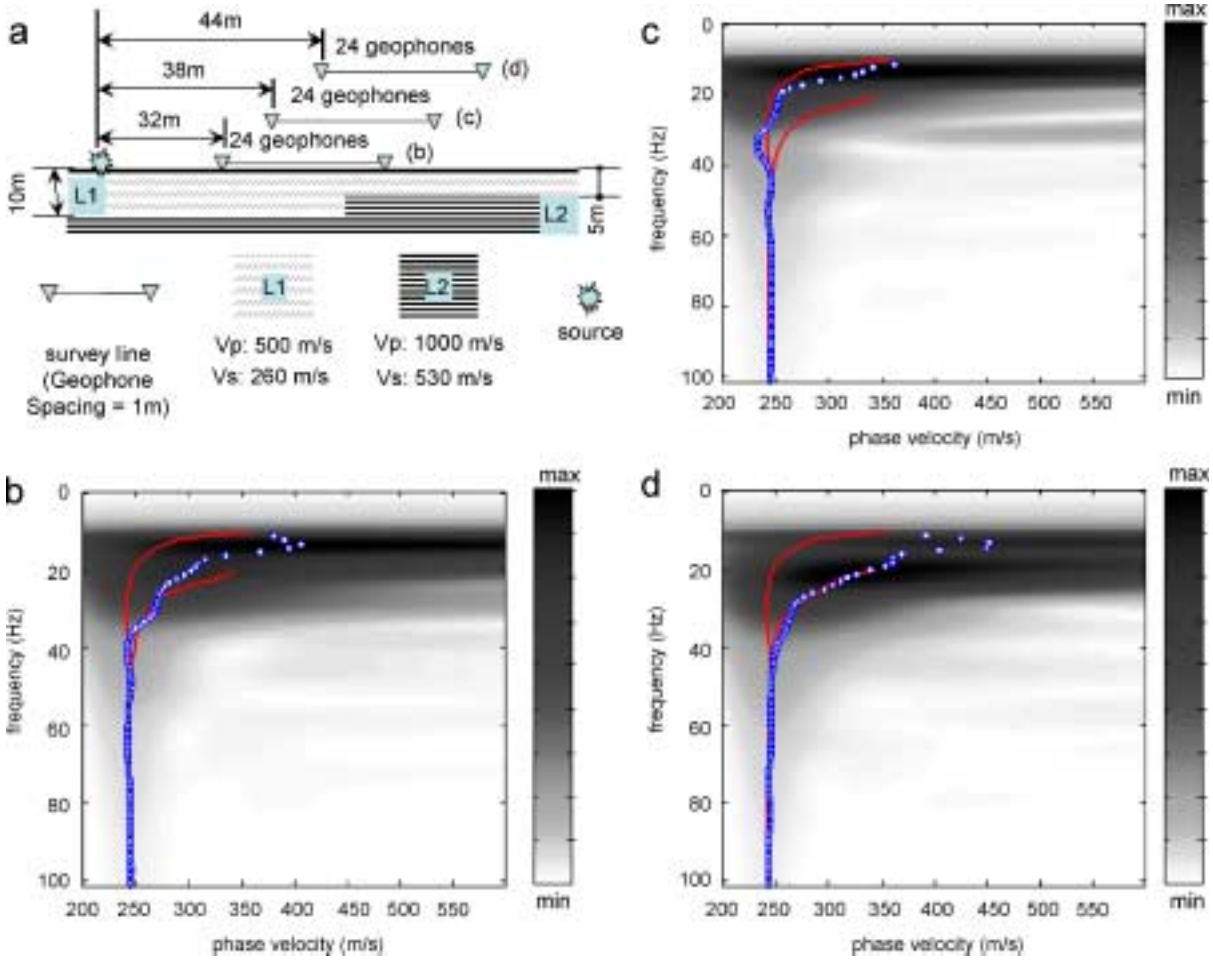

Fig. 5. Effect of lateral heterogeneity on MASW dispersion analysis (a) three cases of geophone spread near the vertical step of the two-layer step structure (b–d) f–v amplitude spectra for each case.

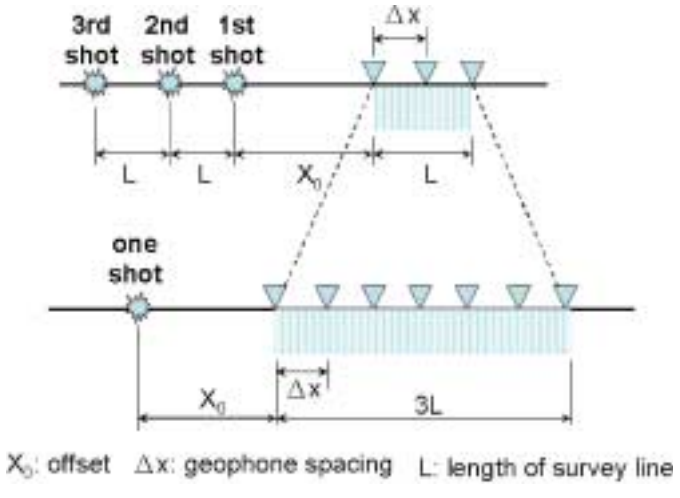

Fig. 6. Illustration of the high-lateral-resolution surface wave method.

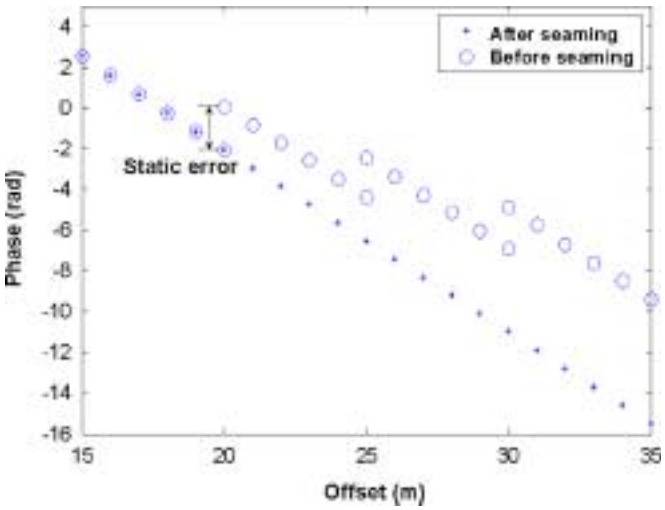

Fig. 7. Unwrapped phase angle at f = 65 Hz vs. source-to-receiver offset for Case a shown in Fig. 8a, illustrating the "phase-seaming procedure" associated with the high-lateral-resolution surface wave method.

delays due to lateral heterogeneity (i.e. lateral variation in Rayleigh-wave velocity). This can be observed from Fig. 9a (the synthetic seismogram for the case shown in Fig. 8a) that the last trace of the first shot and the first trace of the second shot have different arrival times in S-wave packets.

If simply synthesizing the seismic records according to the source-to-receiver offset, a static phase error may be induced between different shots. This is illustrated by the

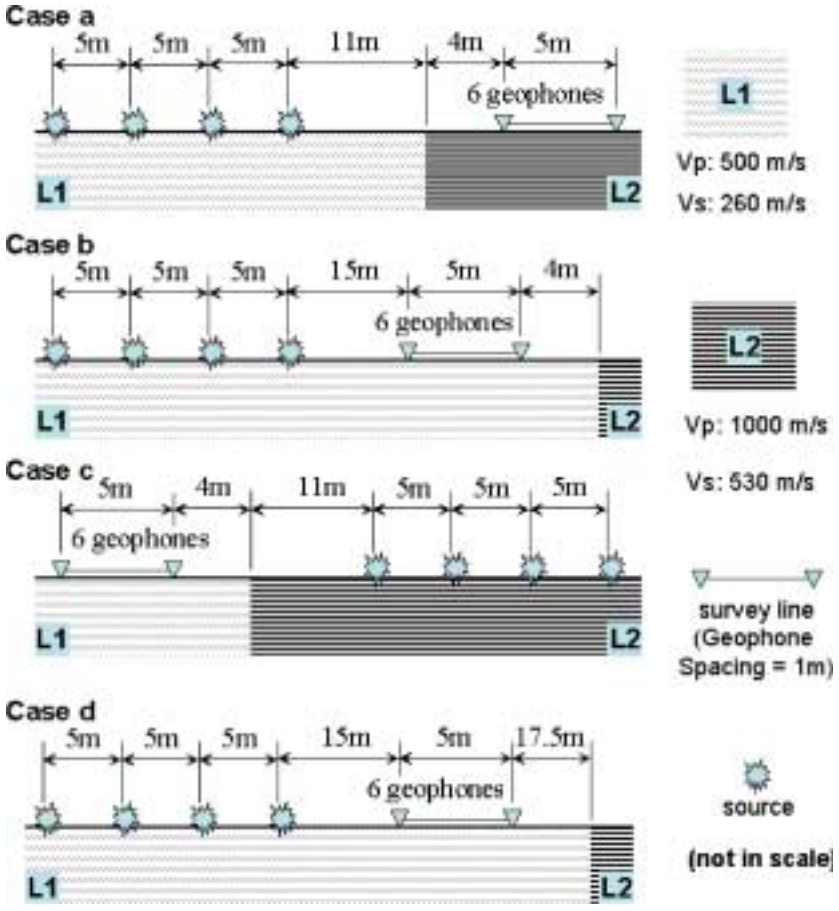

Fig. 8. Various cases used for numerical simulations of the high-lateral-resolution surface wave method in the two-layer vertical structure.

circles in Fig. 7, in which the unwrapped angles are plotted against source-to-receiver offset for frequency $f = 65$ Hz. The lateral heterogeneity results in a phase difference in the same source-to-receiver offsets of two consecutive shots. This static error is in general frequency dependent. An additional data reduction procedure associated with the high-lateral-resolution S-wave method is required when static errors are present. At each frequency, the static phase error between the last waveform of the preceding shot and the first waveform of the subsequent shot is first determined. The static error is then deducted from all traces of the subsequent shot. By doing so, the static error can be corrected as shown by the asterisks in Fig. 7. This data reduction procedure is named as the "phase-seaming procedure." It is applied when static errors occur.

The length of survey line L and the nearest source-to-receiver offset X_0 are two most intangible but important parameters in a conventional field configuration due to near-field effect, far-field effect, and multiple modes. Using the high-lateral-resolution S-wave method, one can determine the Δx according to the shallowest depth of interest and let $X_0 = \Delta x$. The lateral spatial resolution of interest then determines the parameter L. The field survey gathers as many walk-away shots as possible depending on the space available and S-wave attenuation. The high-lateral-resolution S-wave method reduces the effect of lateral heterogeneity while maintaining the resolution and depth range of dispersion analysis. It establishes an expansive offset range in the same spatial range by synthesizing seismic records with different nearest source-to-receiver offsets.

3.3. Numerical simulation of high-lateral-resolution surface wave method

To assess the effectiveness of the high-lateral-resolution S-wave method, a few examples shown in Fig. 8 for the two-layer vertical structure and in Fig. 10 for the two-layer step structure were numerically simulated. In these cases, the geophone spread consists of 6 geophones with 1-m geophone spacing, resulting in only 5 m of offset range in a single shot. Different locations of geophone spread and seismic source are chosen to test the performance in different scenarios. As shown in Figs. 8 and 10, Case a and b represents the geophone spread near the vertical interface but on different sides; Case b and c are used to investigate the effect of shot direction; Case b and d are related to the distance of the geophone spread from the vertical interface. Nine shots were used and the resultant synthesized geophone spread is 45 m.

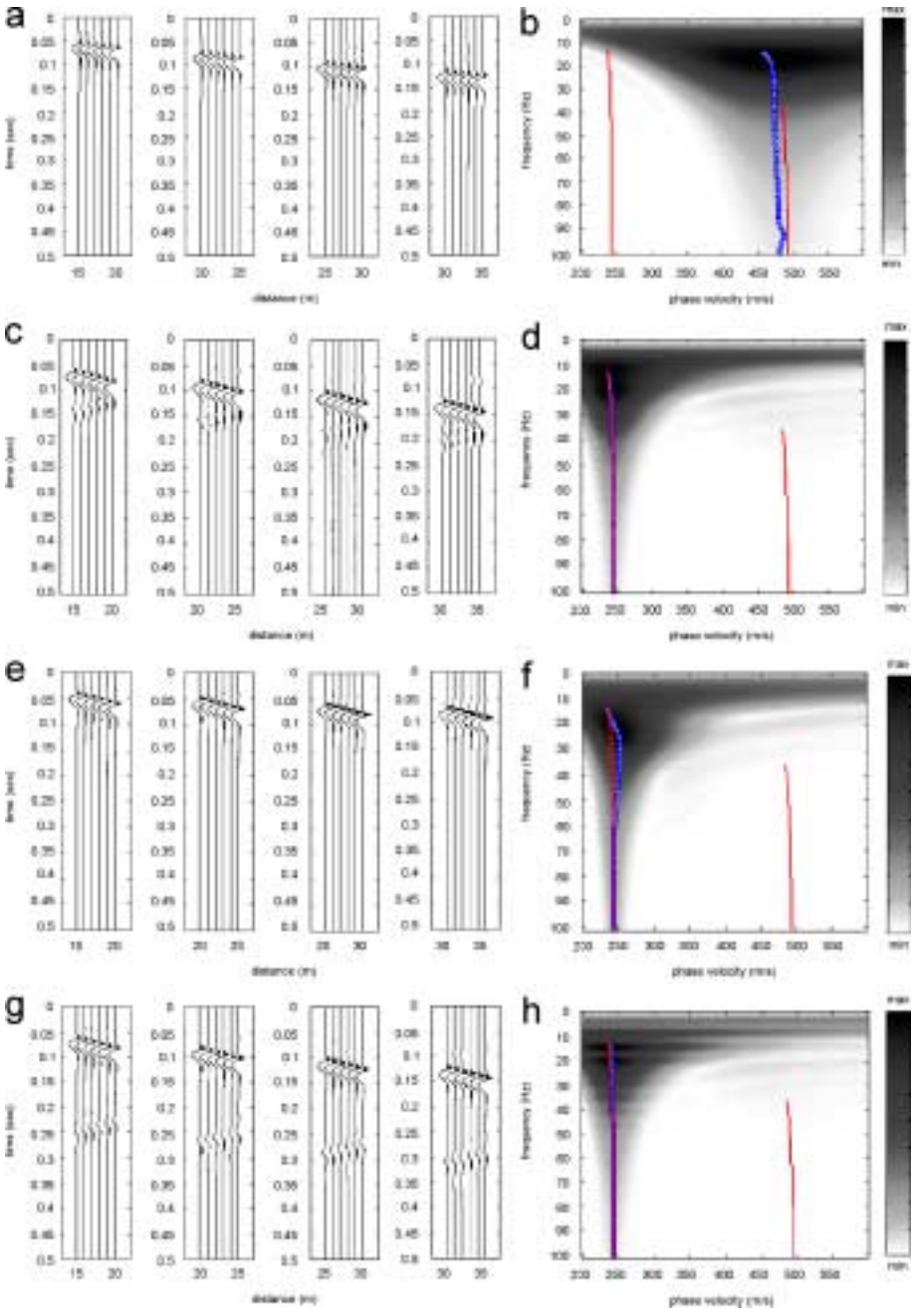

Fig. 9. Synthetic shot gathers and f–v amplitude spectra from the synthesized records for (a, b) Case a, (c, d) Case b, (e, f) Case c, and (g, h) Case d of the two-layer vertical structure.

Fig. 9 shows the first four shot gathers and the f–v magnitude spectra of the synthesized records for Case a, b, c, and d of the two-layer vertical structure. The theoretical dispersion curves for each of the vertical layer are represented by solid lines and the experimental dispersion curve represented by circles. The frequency range selected to represent the theoretical dispersion curve is based on the frequency range that is not affected by numerical dispersion. By applying the high-lateral-resolution S-wave method, the experimental dispersion curve is much more representative of the dispersion characteristics of the stratum beneath the 5 m geophone spread. Some differences still occur when the sources and receivers are on different sides with respect to the interface, as shown in Case a and c. The differences may be explained by the near field effect. In these cases, the first geophone is only 4 m away from the vertical interface even though sources are at least 15 m away. The vertical interface acts as a new source location, causing near field effect to the experimental dispersion curve. The near field effect in Case a is more prominent than in Case c because the layer underneath the geophone spread in Case a has a higher velocity and hence larger wavelength than in Case c. In Case b and d, where the sources and receivers are on the same side with respect

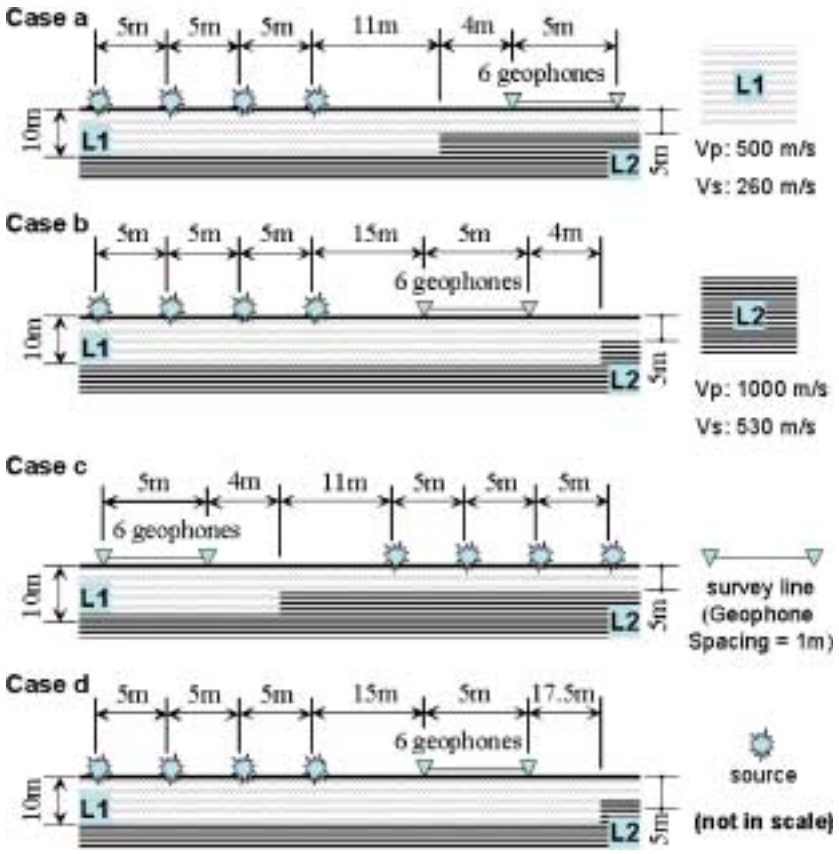

Fig. 10. Various cases used for numerical exercises of the high-lateral-resolution surface wave method in the two-layer step structure.

to the interface, the experimental dispersion curves match the theoretical values extremely well. The result is not affected by the distance between the geophone spread and the interface. The spatial resolution is therefore enhanced by applying the high-lateral-resolution S-wave method.

Similarly, Fig. 11 shows the first four shot gathers and the f–v magnitude spectra of the synthesized records for Case a, b, c, and d of the two-layer step structure. Using the high-lateral-resolution S-wave method, the dispersion curves obtained for all four cases correctly reflect the dispersion curve of the earth structure underneath the 5 m geophone spread. Some discrepancy is noted for Case c, which may be explained by the near field effect due to diffraction at the corner edge. As shown in Figs. 9 and 11, both exercises demonstrate that the high-lateral-resolution S-wave method can greatly alleviate the effect of lateral heterogeneity and increase spatial resolution. When the conventional MASW method is used, a long geophone spread is required to have enough depth coverage. A large area will be affected by the lateral heterogeneity, as shown in Figs. 3 and 5. On the contrary, only a small area is affected by the lateral heterogeneity in the high-lateral-resolution S-wave method. It should be noted that, however, results similar to Figs. 3 and 5 will be obtained when the short survey line is right across the vertical structures. This implies that there is an abrupt lateral variation of earth structure within that short distance. In most cases, the assumption of a horizontally layered medium is better justified when the geophone spread is within a small range.

4. Conclusions

MASW has been increasingly used to map not only the vertical variation but also the lateral variation of S-wave velocity ignoring the assumption of a horizontally layered medium. This paper discusses the effect of lateral heterogeneity on the conventional dispersion analysis of S-wave by means of numerical simulations. Results show that the lateral heterogeneity induces a non-stationary property in the space domain, resulting in false depth-related dispersion or higher modes if conventional approach based on stationary assumption is used for the dispersion analysis. When making usual assumption of a horizontally layered medium during inversion, the lateral variation of S-wave velocity will be falsely recognized as the vertical variation, hence introducing artifacts in 2-D S-wave velocity imaging. A countermeasure, named here the high-lateral-resolution S-wave method, is proposed to reduce the effect of lateral heterogeneity while maintaining the resolution and depth range of dispersion analysis. It consists of a walk-away survey and a phase-seaming procedure for allowing wide-wavelength dispersion analysis within a small spatial range. The sources and receivers are deployed in such a way that

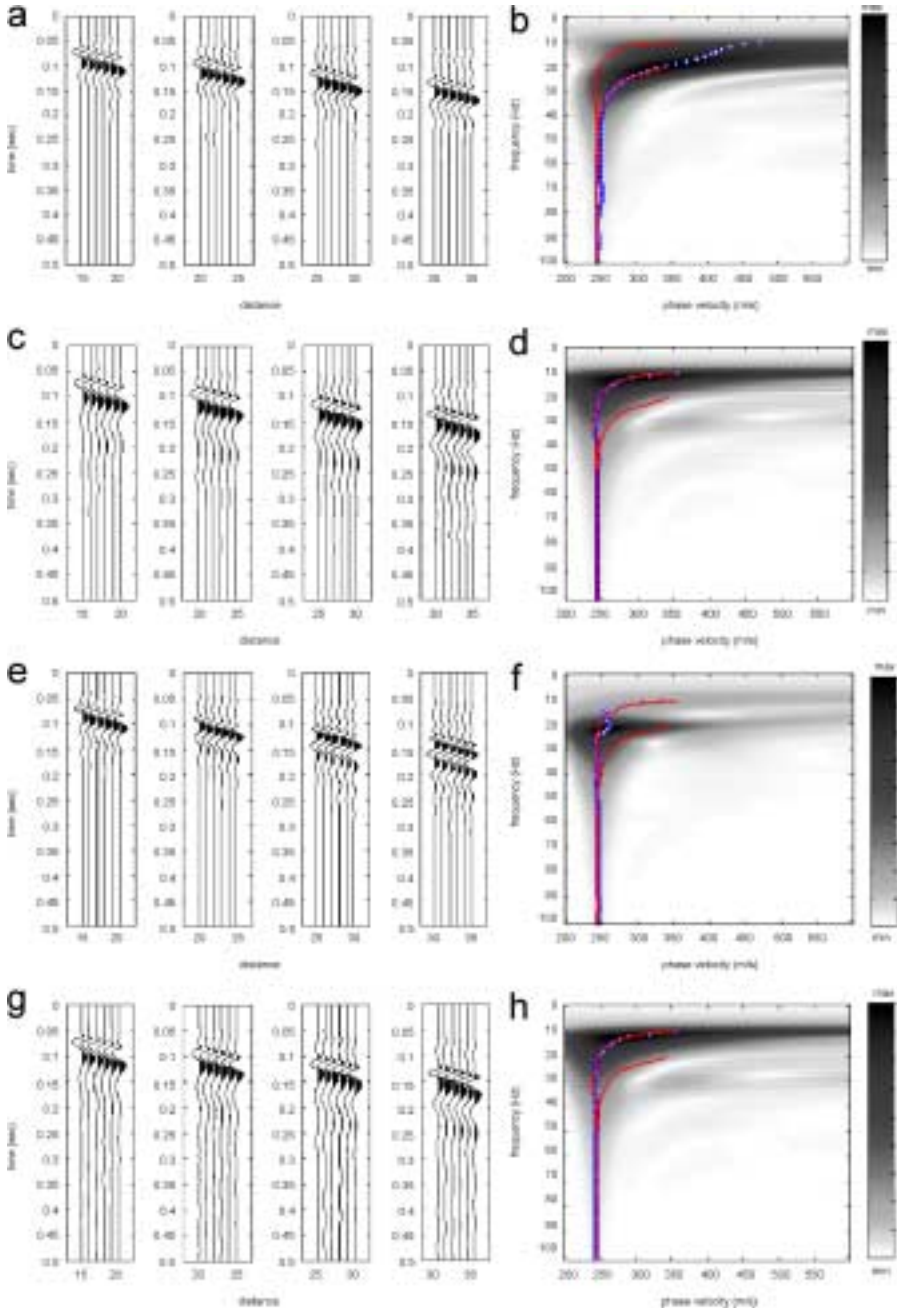

Fig. 11. Synthetic shot gathers and f–v amplitude spectra from the synthesized records for (a, b) Case a, (c, d) Case b, (e, f) Case c, and (g, h) Case d of the two-layer step structure.

the farthest source-to-receiver offset of the preceding shot is equal to the nearest source-to-receiver offset of the subsequent shot. A phase-seaming procedure is devised to correct potential static errors when synthesizing the seismic records with different nearest source-to-receiver offsets. Numerical simulations show that the high-lateral-resolution S-wave method can greatly alleviate the effect of lateral heterogeneity and increase spatial resolution. As a first attempt to clearly illustrate the effect of lateral heterogeneity, the earth model used in this study maybe over simplified. Other more complex cases will be investigated in future studies. The high-lateral-resolution S-wave method still assumes a horizontally layered medium. It may be a time to start thinking in terms of direct 2-D modeling and inversion in S-wave testing applications.

Acknowledgments

This research is supported in part by the National Science Council of ROC under Contract No. 93-2211-E-009-013 and the MOU-ATU program. These supports are greatly appreciated. Suggestions of anonymous reviewers improved the paper.

References

[1] Socco LV, Strobbia C. Surface-wave method for near surface characterization: a tutorial. Near Surface Geophys 2004;2:165–85.

[2] Stokoe II KH, John SH, Woods RD. Some contributions of in situ geophysical measurements to solving geotechnical engineering problems. In: Proceedings of second international conference on site characterization, vol. 1, Porto, Portugal, 2004, p. 97–132.

[3] Foti S. Small-strain stiffness and damping ratio of Pisa clay from surface wave tests. Geotechnique 2003;53:455–61.

[4] Lin C-P, Chang C-C, Chang T-S. The use of MASW method in the assessment of soil liquefaction potential. Soil Dynam Earthquake Eng 2004;24:689–98.

[5] Gucunski N, Krstic V. Backcalculation of pavement profiles from spectral-analysis-of-surface-waves test by neural networks using individual receiver spacing approach. Transport Res Rec 1996;1526: 6–13.

[6] Ryden N, Park CB, Ulriksen P, Miller RD. Multimodal approach to seismic pavement testing. J Geotech Geo-Environ Eng 2004;130: 636–45.

[7] Andrus R, Chung R, Stokoe II KH, Bay J. Delineation of densified sand at Treasure Island by SASW testing in geotechnical site characterization. In: Proceedings of the first international conference on site characterization (ISC'98), vol. 1, Atlanta, USA, 1998, p. 459–64.

[8] Rix GJ, Lai CG, Foti S, Zywicki D. Surface wave tests in landfills and embankments. ASCE Geotech Special Publ 1998(75):1008–19.

[9] Haegeman W, Van Impe WF. Characterization of disposal sites from surface wave measurements. J Environ Eng Geophys 1999;4:27–33.

[10] Gucunski N, Krstic V, Maher MH. Experimental procedures for detection of underground objects. In: Proceedings of the first international conference on site characterization (ISC'98), vol. 1, Atlanta, USA, 1998, p. 469–72.

[11] Nazarian S, Stokoe II KH. In situ shear wave velocities from spectral analysis of surface waves. In: Proceedings of eighth conference on earthquake engineering, vol. 3, San Francisco, 1984, p. 38–45.

[12] Stokoe II KH, Wright SG, Bay JA, Roesset JM. Characterization of geotechnical sites by SASW method. In: Woods RD, editor. Geophysical characterization of sites. Rotterdam: Balkema; 1994. p. 15–25.

[13] Tokimatsu K. Geotechnical site characterization using surface waves. In: Proceedings of the first international conference on earthquake geotechnical engineering, Tokyo, Japan. Rotterdam: Balkema; 1995. p. 1333–68.

[14] Park CB, Miller RD, Xia J. Multichannel analysis of surface waves. Geophysics 1999;64:800–8.

[15] Xia J, Miller RD, Park CB. Estimation of near-surface shear-wave velocity by inversion of Rayleigh wave. Geophysics 1999;64: 691–700.

[16] Foti, S. Multistation methods for geotechnical characterization using surface waves. PhD dissertation, Politecnico di Torino, 2000.

[17] Lin CP, Chang TS. Multi-station analysis of surface wave dispersion. Soil Dynam Earthquake Eng 2004;24:877–86.

[18] Miller RD, Xia J, Park CB, Ivanov J. Multichannel analysis of surface waves to map bed rock. Leading Edge 1999;18:1392–6.

[19] Sheehan J, Doll W, Mandell W. Comparison of MASW and refraction tomography. In: Symposium on the application of geophysics to engineering and environmental problems, Colorado Springs, Colorado, 2004, p. 1611–21.

[20] Xia J, Chen C, Li PH, Lewis MJ. Delineation of a collapse feature in a noisy environment using a multichannel surface wave technique. Geotechnique 2004;54:17–27.

[21] Dayakar P, Park CB. Multichannel analysis of surface wave (MASW) method for geotechnical site characterization. ASCE Geotech Special Publ 2005(133):957–66.

[22] Thitimakorn T, Anderson NL, Stephenson R, Liu W. 2-D shear-wave velocity profile along test segment of Interstate I-70, St. Louis, Missouri. ASCE Geotech Special Publ 2005(138):2159–67.

[23] Levander AR. Fourth-order finite-difference P-SV seismograms. Geophysics 1988;53:1425–36.

[24] Robertsson JOA. A numerical free-surface condition for elastic/viscoelastic finite-difference modeling in the presence of topography. Geophysics 1996;61:1921–34.

[25] Cerjan C, Kosloff D, Kosloff R, Reshef M. A nonreflecting boundary condition for discrete acoustic and elastic wave equations. Geophysics 1985;50:705–8.

[26] McMechan GA, Yedlin MJ. Analysis of dispersive waves by wave-field transformation. Geophysics 1981;46:869–74.

[27] Gabriels P, Snieder R, Nolet G. In situ measurements of shear-wave velocity in sediments with higher-mode Rayleigh waves. Geophys Prospecting 1987;35:187–96.

[28] Park CB, Miller RD, Xia J. Imaging dispersion curves of surface waves on multi-channel record. In: 68th annual international meeting, Society of Exploration Geophysicists, Expanded Abstracts, 1998, p. 1377–80.

[29] Prokis JG, Manolakis DG. Digital signal processing—principles, algorithms, and applications. 3rd ed. Englewood Cliffs, NJ: Prentice-Hall; 1992.